

A Gigaparsec-Scale Hydrodynamic Volume Reconstructed with Deep Learning

COOPER JACOBUS,^{1,2} SOLENE CHABANIER,¹ PETER HARRINGTON,¹ JD EMBERSON,³ ZARIJA LUKIĆ,¹ AND SALMAN HABIB³

¹*Lawrence Berkeley National Laboratory, Berkeley, CA 94720, USA*

²*Department of Astronomy, University of California, Berkeley, CA 94720, USA*

³*Argonne National Laboratory, Lemont, IL 60439, USA*

ABSTRACT

The next generation of cosmological spectroscopic sky surveys will probe the distribution of matter across several Gigaparsecs (Gpc) or many billion light-years. In order to leverage the rich data in these new maps to gain a better understanding of the physics that shapes the large-scale structure of the cosmos, observed matter distributions must be compared to simulated mock skies. Small mock skies can be produced using precise, physics-driven hydrodynamical simulations. However, the need to capture small, kpc-scale density fluctuations in the intergalactic medium (IGM) places tight restrictions on the necessary minimum resolution of these simulations. Even on the most powerful supercomputers, it is impossible to run simulations of such high resolution in volumes comparable to what will be probed by future surveys, due to the vast quantity of data needed to store such a simulation in computer memory. However, it is possible to represent the essential features of these high-resolution simulations using orders of magnitude less memory. We present a hybrid approach that employs a physics-driven hydrodynamical simulation at a much lower-than-necessary resolution, followed by a data-driven, deep-learning Enhancement. This hybrid approach allows us to produce hydrodynamic mock skies that accurately capture small, kpc-scale features in the IGM but which span hundreds of Megaparsecs. We have produced such a volume which is roughly one Gigaparsec in diameter and examine its relevant large-scale statistical features, emphasizing certain properties that could not be captured by previous smaller simulations. We present this hydrodynamic volume as well as a companion n-body dark matter simulation and halo catalog which we are making publically available to the community for use in calibrating data pipelines for upcoming survey analyses.

Keywords: Cosmology (343); Intergalactic medium (813); Large-scale structure of the universe (902); Lyman alpha forest (980); Convolutional neural networks (1938)

1. INTRODUCTION

The vast space between clusters of galaxies is filled with a rich and complex web-like structure of gas. While this gas is not dense enough to form stars and thus does not emit much light, it absorbs light and its presence imprints itself in the spectra of distant quasars as their light passes through these clouds en route to earth. The web-like structure of the gas produces a characteristic pattern in the quasars absorption spectra called the Lyman-*alpha* forest. The distribution of the absorption line reflects the distribution and thermal properties of the intervening gas, which is shaped by the expansion history of the cosmos, among other phenomena (for a recent review, see McQuinn (2016)).

A survey of hundreds of thousands of these quasar spectra will reflect the distribution of the matter in the cosmos and can be used to infer the nature of the physics

that produced the underlying structure. The aggregate 1-dimensional power spectrum (P1D) of these absorption maps along the lines of sight can be used to constrain properties of the local universe as a whole (Croft et al. 1999; McDonald et al. 2005; Palanque-Delabrouille et al. 2013; Chabanier et al. 2019; Karaçaylı et al. 2022), and have been shown to provide excellent constraints on the sum of neutrino masses (Seljak et al. 2005; Palanque-Delabrouille et al. 2015a,b; Palanque-Delabrouille et al. 2019) and the nature of dark matter (Viel et al. 2005, 2013; Baur et al. 2017; Yèche et al. 2017; Iršič et al. 2017; Armengaud et al. 2017; Dvorkin et al. 2014; Xu et al. 2018; Garny et al. 2018). But the Ly- α forest can be leveraged to even greater effect by using the 3-dimensional power spectrum, which captures the correlations both along and perpendicular to the line of sight and thus vastly expands the number of available modes

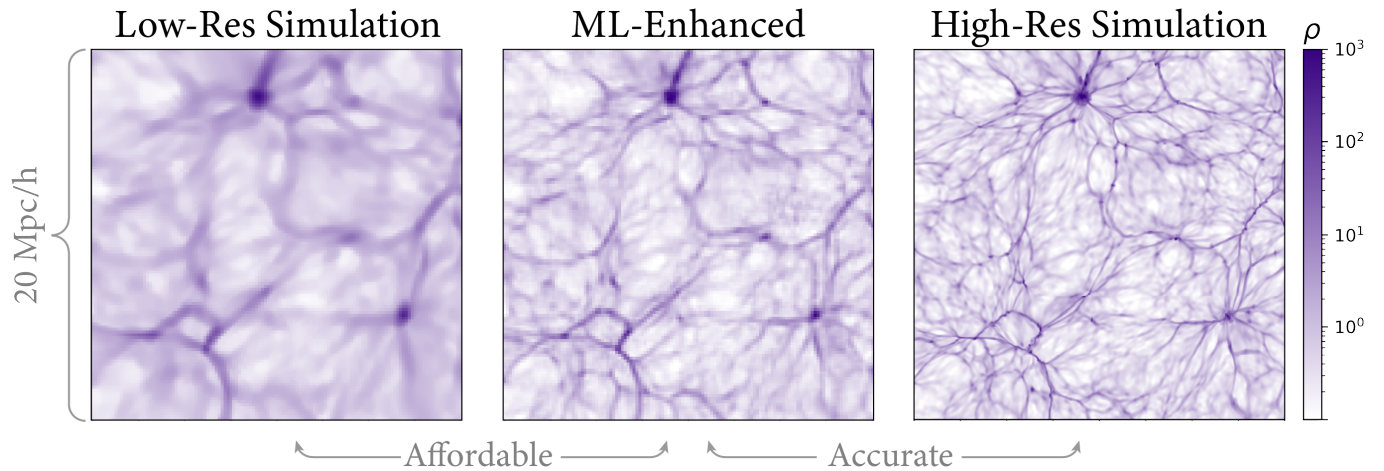


Figure 1. Comparison of simulated and predicted Hydrodynamic density fields, visualized in log-space relative to the mean density. The left panel is the low-resolution simulation which is fed as input to our model. The center panel is the map reconstructed by our machine-learning model, which is trained to match features from the high-resolution simulation in the right panel. Our model demonstrates a clear improvement over the low-resolution simulation.

(see Rorai et al. (2017)). This offers the possibility to better constrain cosmological parameters. Measurement of the 3D powerspectrum of the Ly- α forest has not yet been made, because it requires a very large survey volume and a very large number of lines of sight. However, the ongoing survey by the Dark Energy Spectroscopic Instrument (DESI Collaboration et al. 2016) will make this measurement possible and a future 5th-generation Spectroscopic survey is already being designed by the cosmological community (Chou et al. 2022), which will further improve the precision of such measurement.

Large spectroscopic surveys also enable cross-correlating Ly- α and other tracers of matter fluctuations. For instance correlating with CMB lensing will allow us to probe nonlinear structure formation at large scales during periods on cosmic history that are otherwise hard to examine (Vallinotto et al. 2011; Chiang & Slosar 2018; Dash & Guha Sarkar 2021). Or correlating with galaxy positions may allow us to improve our reconstructions of the initial conditions of the universe.

Performing this cosmological inference requires not only vast surveys of precise observations, but also accurate theoretical modeling of the structure of the universe. There is no analytic solution for the evolution of density fluctuations in the universe on the scale of galaxy clusters, so it is necessary to model the state of the IGM numerically. These hydrodynamic cosmological simulations provide a consistent description of the IGM in the context of the formation of large scale structure (Cen et al. 1994), but can be very computationally expensive. In order to accurately model the Ly- α forest, they must be able capture small-scale fluid behavior and thus need to resolve density fluctuations in the IGM on the scale of ~ 20 kpc/h (Lukić et al. 2015; Walther et al. 2021;

Chabanier et al. 2023; Doughty et al. 2023) even though observatories like DESI can measure these fluctuations only at scales $\gtrsim 1$ Mpc/h (Karaçaylı et al. 2023; Ravoux et al. 2023) (see figure 9). This imposes a stringent limitation on the maximum size of the volumes that can be produced, for example, a 1 Gpc/h simulation would require over a Petabyte of memory, far beyond the resources of even the most modern supercomputers.

Recently, machine learning has shown remarkable potential for reducing the computational expense of solving these highly non-linear problems by serving as a surrogate model for complex physics simulations (for a recent review of many deep learning applications in cosmology, see Huertas-Company & Lanusse (2023)). We have developed a method for producing mock skies using a significantly lower memory footprint (Jacobus et al. 2023). Our novel approach uses conditional generative adversarial networks (Goodfellow et al. 2014; Mirza & Osindero 2014) and is trained on pairs of hydrodynamic simulations. This allows us to perform much cheaper and more memory-efficient low-resolution simulations and correct them to better resemble higher-resolution simulations that would be infeasible to run for large volumes. In this work, we apply our model to a hydrodynamical simulation nearly a Gigaparsec in diameter.

This paper is organized as follows. We first discuss the simulations we use to train our network in Section 2. We then briefly outline the design and novelty of our deep-learning algorithm and the methods used to train it in section 3. Our results are presented in Section 4, where we discuss the accuracy of our algorithm and explore some of the statistical features of our new Gpc-scale volume. Finally, we present conclusions and an outlook on future work in Section 5.

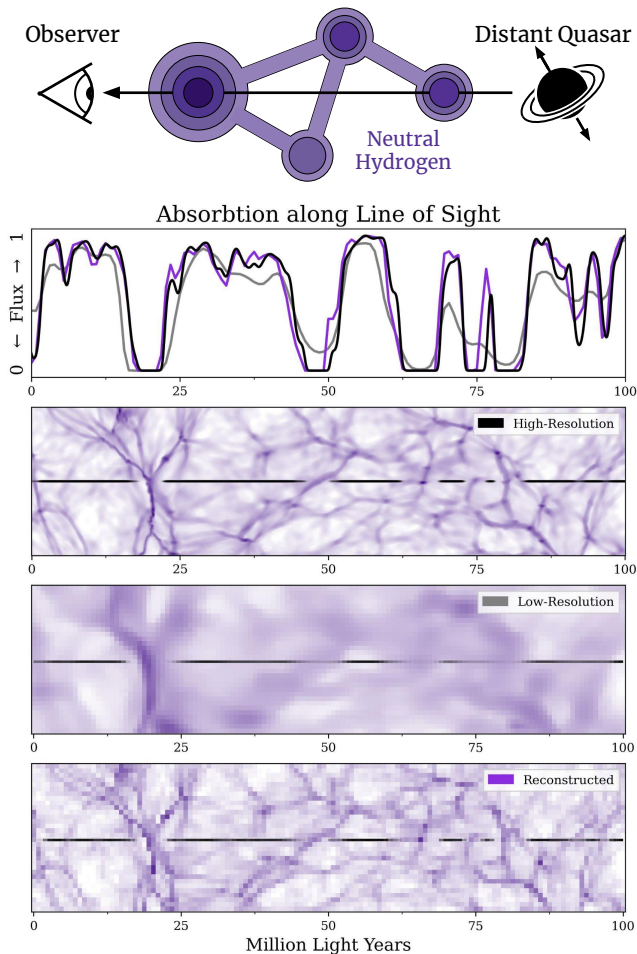


Figure 2. Illustration of the effects of resolution on simulated Lyman- α absorption features. We plot slices of Baryon Density 10^8 ly (~ 30 Mpc) wide for High-Res, Low-Res, and Reconstructed fields. We plot sample lines of sight through these fields and show the (non-redshifted) Lyman- α flux above. Notice that absorption features are spectrally sharpest in the high-resolution simulation but that some spectral detail is returned by our reconstructed field.

2. TRAINING DATA

We assemble our training and testing data from pairs of simulations run by the publicly available *Nyx* code (Almgren et al. 2013; Sexton et al. 2021). The code follows the evolution of dark matter using collisionless self-gravitating Lagrangian particles which are coupled to baryonic ideal gas modeled on a uniform Cartesian grid. Although *Nyx* is capable of employing adaptive mesh refinement (AMR), we do not make use of this functionality here as the Ly- α signal spans the vast low-density volumes and is fully absorbed close to halos where AMR would be relevant. To model the Lyman α forest, *Nyx* models primordial gas composition of neutral and ionized Hydrogen and Helium, as well as free electrons.

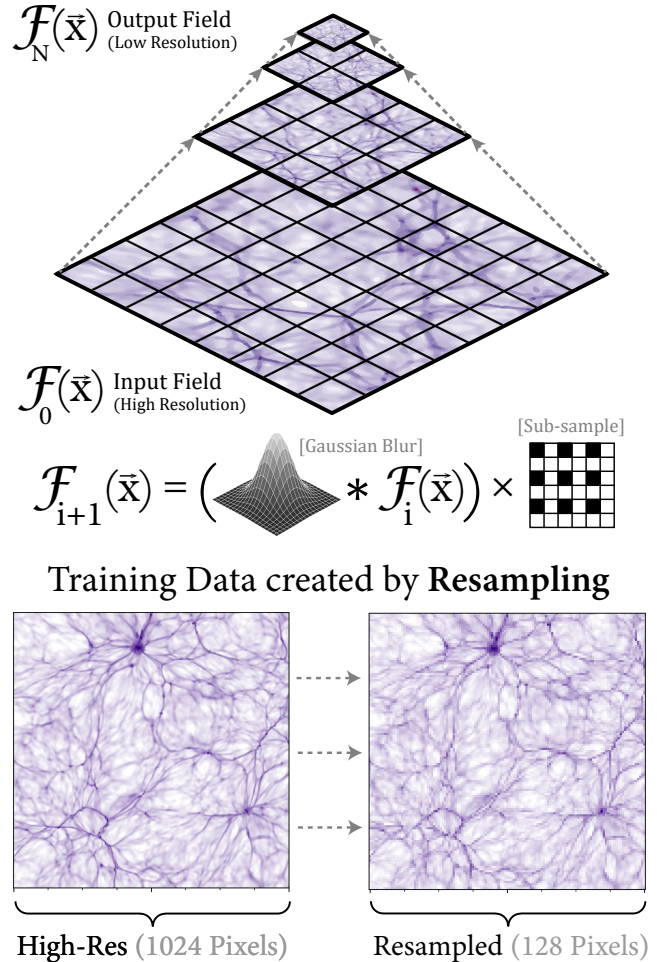
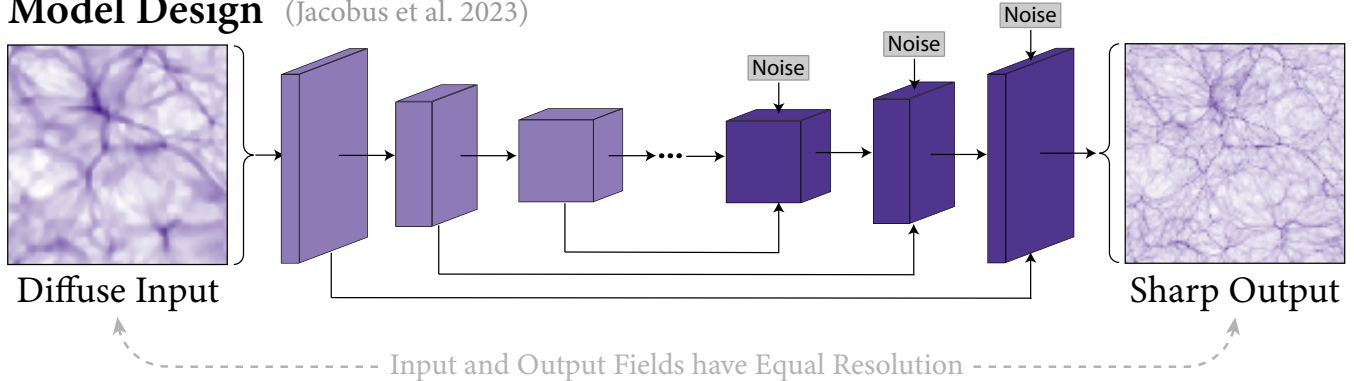


Figure 3. Illustration of the process for creating training data target fields from high-resolution simulations. Fields are iteratively Gaussian blurred and sub-sampled until they match the grid size (and data footprint) of the low-resolution simulations. This method preserves most fine structures while dramatically reducing the memory necessary to store the density fields on our computer.

This type of simulation is very common in studies of the intergalactic medium and is used as a forward model in virtually any recent inference work using the Lyman alpha power spectrum (Boera et al. 2019; Walther et al. 2019; Palanque-Delabrouille et al. 2020; Rogers & Peiris 2020; Walther et al. 2021).

The simulations are initialized at $z = 200$, using the Zel'dovich approximation (Zel'dovich 1970). Transfer functions were generated with the Boltzmann solver code CLASS (Blas et al. 2011). The cosmological parameters are set according to the Planck-2016 (Planck Collaboration et al. 2016) model: $\Omega_b = 0.0487$, $\Omega_m = 0.31$, $H_0 = 67.5$, $n_s = 0.96$ and $\sigma_8 = 0.83$. For our training data, we produce two pairs of simulations $80 h^{-1}$ Mpc on a side, where each pair has a high- and

Model Design (Jacobus et al. 2023)



Application to Large Volume

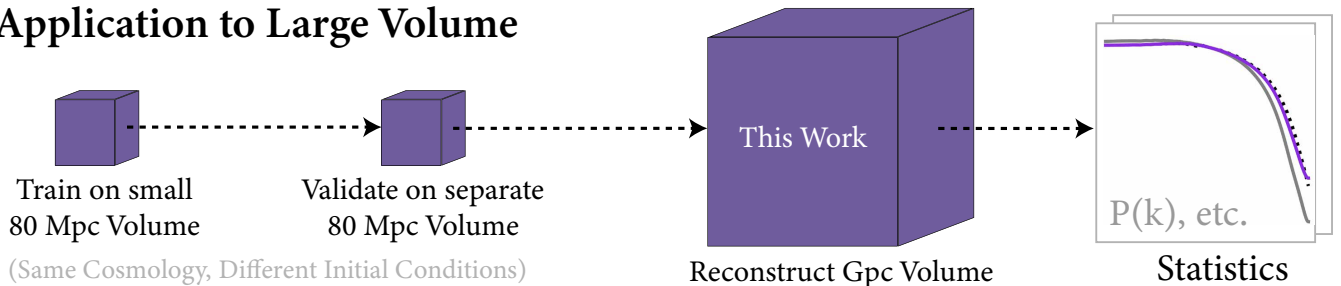


Figure 4. (Top) Flowchart showing a rough sketch of the architecture of our custom machine learning model which improves the realization and spectral accuracy of features in low-resolution hydrodynamic simulations. (Bottom) Illustration of the training and inference pipeline, noting the substantial difference in size between our training and inference volumes.

low-resolution run initialized from the same random initial conditions. The high-resolution simulations have 4096^3 elements (particles and grid cells) and are thus fully converged and percent-level accurate, while the low-resolution simulations are much coarser with only 512^3 elements. All simulation runs have identical cosmology, UV background, and all numerical parameters, and the two pairs of high- and low-resolution simulations differ only in the choice of random realization. This enables the model to be trained on one pair of simulations and tested on another. We use the software suite `gimlet` (Friesen et al. 2016) to derive the optical depth and flux fields from our hydrodynamic fields.

2.1. Resampling and the Gaussian Pyramid

In order to generate training data of high spectral fidelity but with a resolution equal to our inexpensive simulations, we use an iterative blurring and resampling method known as a Gaussian pyramid (Meer et al. 1987). We wish to reduce the data footprint of our high-resolution simulations by a factor of 512 while preserving the field’s spectral information. We achieve this by iteratively applying a Gaussian blur and subsampling our fields by a factor of 2, as depicted in figure 3. We describe this method in more detail and demonstrate that it prevents aliasing in (Jacobus et al. 2023).

3. MODEL DESIGN

Modeling hydrodynamic fields from high-resolution simulations on a coarse grid presents a challenging task for deep learning due to the sharp features and uncertainty in the mapping from coarse to fine fields. We have adopted a conditional GAN architecture (Karras et al. 2019, 2020) based on the fully-convolutional TSIT model (Jiang et al. 2020), which uses a multi-scale encoder-generator framework with residual blocks for feature extraction at multiple scales. This design is able to capture both localized features accurately and sample multiple realizations of the target fields, allowing for model uncertainty estimation via ensemble predictions.

To capture uncertainty, we incorporate multi-scale Gaussian noise injection into the generator at all feature resolutions, similar to generators like StyleGAN (Karras et al. 2019). This approach, where injected noise scales are learnable parameters, enhances stochasticity and enables the generation of physically realistic variations in predictions. By injecting noise at different scales, the model captures variability in the finer spatial features, addressing the limitations of single-point noise injection methods. This noise injection method makes it possible to produce an ensemble of subtly different realizations. We demonstrate in (Jacobus et al. 2023) that

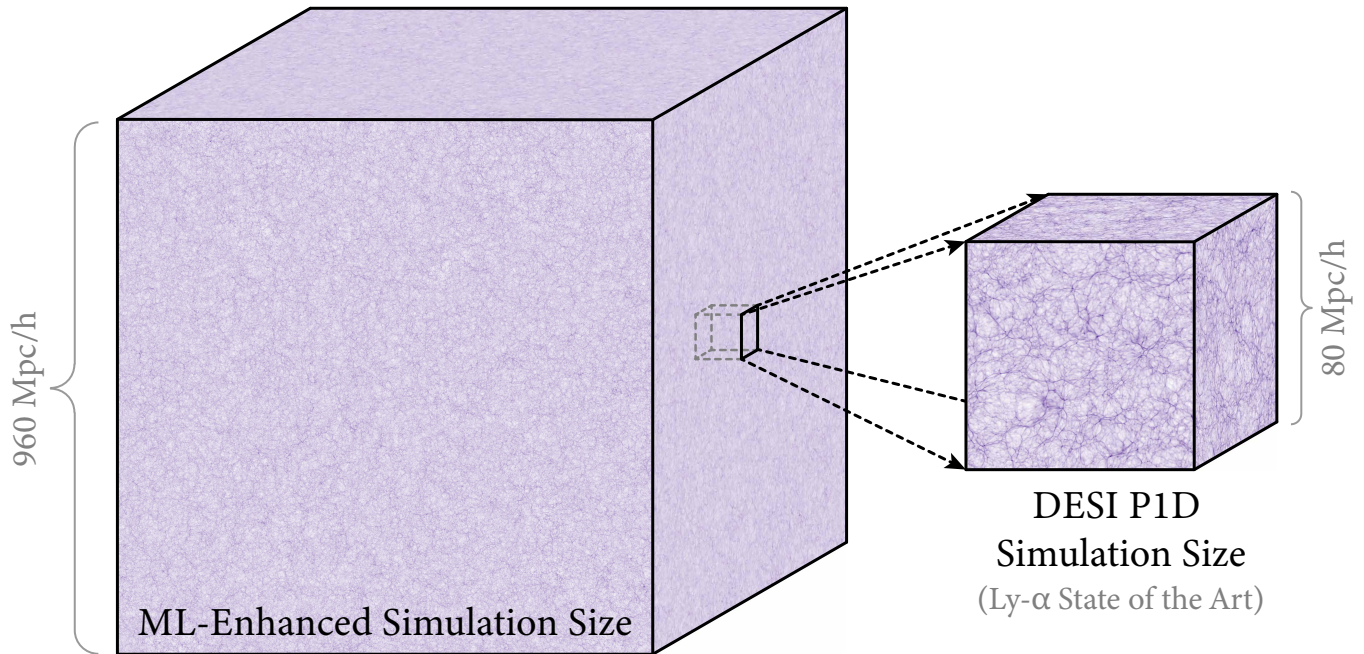


Figure 5. Visualization of the 960 Mpc/h wide Baryon Density volume we have reconstructed using our machine learning model. The dashed box highlights a region 80 Mpc/h wide, which is the size of our training data and comparable to existing traditional simulations used for DESI and other surveys.

the point-wise variation of these ensembles correlates strongly with the point-wise predictive error, allowing us to reliably estimate our model’s prediction uncertainty and propagate it through our analysis pipeline.

The hydrodynamic fields produced by *Nyx* span several orders of magnitude and features in the baryon density and temperature fields, like galaxy clusters and thermal shocks, are most easily interpretable in log-space. Before passing these density and temperature fields into our machine learning model, we log-normalize them such that all cells are mapped to the range $[-1,1]$. To constrain the output fields to their target ranges, we use a hyperbolic tangent filter on the final layer for hydrodynamic fields and a sigmoid filter for Ly- α flux. Hydrodynamic fields are de-normalized before returning the final output, but are trained in log-space.

We employ multiple loss functions to incentivize our networks to reproduce various statistical qualities present in the data. The dominant component of the total loss objective used for training is point-wise \mathcal{L}_1 distance, which encourages large-scale features to match between the predictions and targets, and improves training stability. To encourage the model to capture fine-scale features, we also employ a multi-scale adversarial loss based on (Wang et al. 2018; Park et al. 2019; Jiang et al. 2020), which is defined by multiple patch-based discriminator networks that each see different resized versions of the generated and ground truth data. Fi-

nally, since the spectral statistical accuracy of our output is of utmost importance, we introduce a spectral loss term, \mathcal{L}_{fft} , which is a measure of the difference between the truncated Fourier transforms of the prediction and target. Further details about the design and training of our machine learning architecture, as well as inference techniques, can be found in (Jacobus et al. 2023).

4. SIMULATION RESULTS

We present a new hydrodynamic simulation volume reconstructed using our deep-learning method. The simulation is a cube 960 Mpc/h wide represented by 6144^3 volumetric cells containing values of Dark Matter Density, Baryon Density, Temperature, Velocity, and Lyman- α Optical Depth. Our simulation was run using *Nyx* at a resolution exactly matching that of our low-resolution training data, was likewise initialized at $z = 200$, and with the exact same cosmology ($\Omega_b = 0.0487$, $\Omega_m = 0.31$, $H_0 = 67.5$, $n_s = 0.96$ and $\sigma_8 = 0.83$). We stop the simulation at a redshift of $z = 3$ and then pass it through our deep-learning model to make it more physically realistic on small scales. The receptive field of our convolutional architecture is 32 voxels (or 5 Mpc/h), so we can reconstruct our large volume in small, 20 Mpc/h wide chunks using many GPUs in parallel. The entire 960 Mpc/h simulation file requires only 11 Terabytes of computer memory, including all of the representations of dark matter, baryons, and the Lyman- α optical depth.

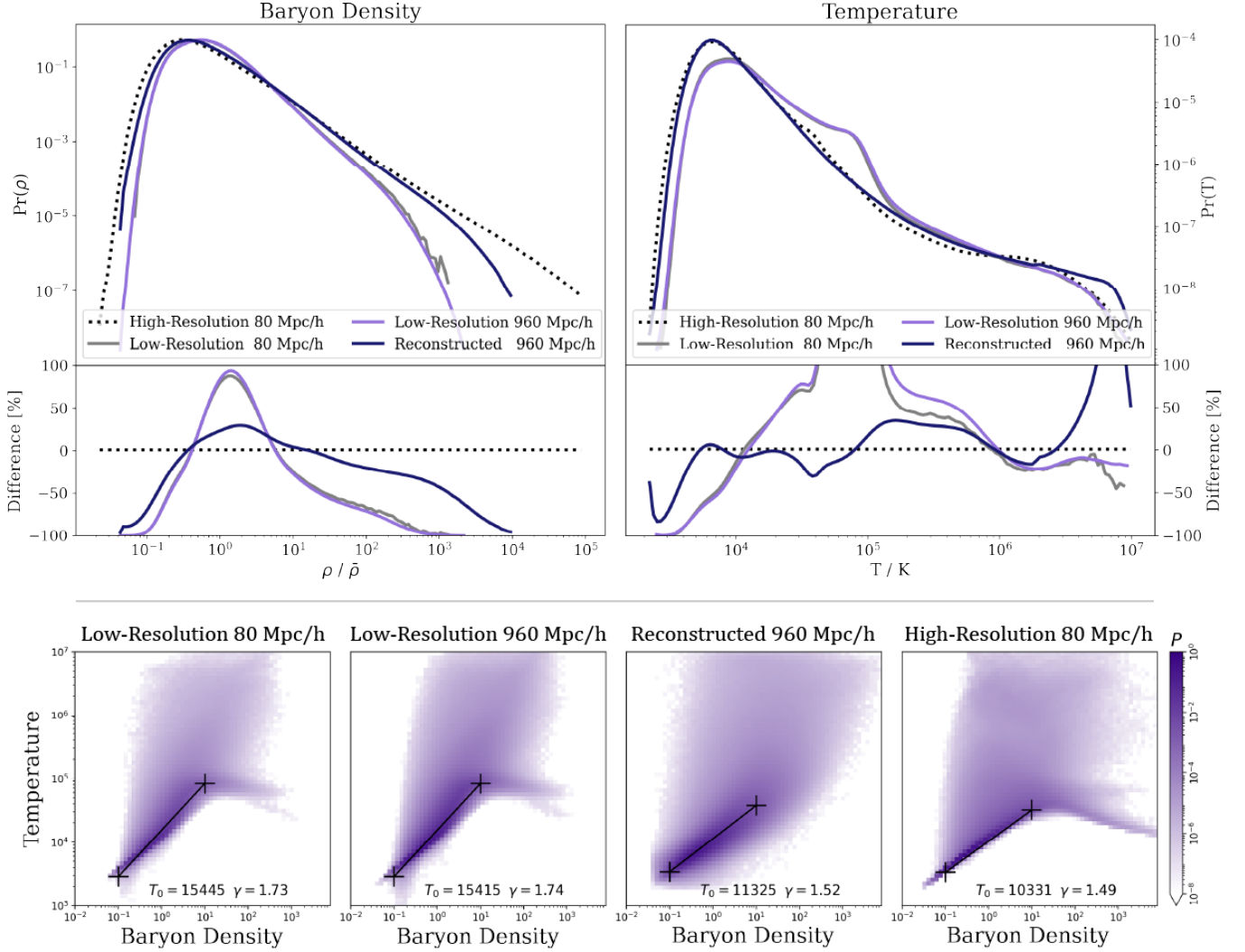


Figure 6. (Top) The Probability Density Functions of the predicted density and temperature fields compared against the reference distributions from a target high-resolution simulation. (Bottom) The density–temperature distribution of the gas in our model prediction compared against the reference distributions from the low-resolution and high-resolution simulations. For each output we plot the best-fit power-law relationship between density and temperature, our model presents an improvement in the slope of this power-law, γ , when compared against the low-resolution simulation, but produces a much broader distribution.

4.1. Hydrodynamic Fields

The baryon density field of the 960 Mpc/h wide volume we reconstructed by our machine learning model is visualized in figure 5, and the improvement is visually demonstrated in figure 1. We examine the statistical properties of the baryon density and temperature in figure 6. We compare the probability distributions of our baryon density and temperature to those from a ‘true’ high-resolution simulation of a much smaller volume. The output of our machine-learning model presents a clear improvement over the low-resolution simulation volume, both the distribution peaks have been noticeably corrected and the distribution shapes have been adjusted to better match that of the high-resolution base-

line (except for an over-prediction of extreme temperatures, which should not impact the Ly- α signal).

We also plot the 2D Density-Temperature distribution in figure 6. As a result of the downsampling scheme used to generate our targets, much of the diversity in the gas density–temperature distribution is not reproduced by our method. Our resulting volume does not accurately capture the Density-Temperature tail consisting of condensed galaxy-forming regions. However, those regimes are of little consequence for the Ly- α forest and our method does improve the power-law relationship of the diffuse gas, $T = T_0(\rho/\langle\rho\rangle)^{\gamma-1}$, which is more impactful on the Ly- α signal and can provide insights into the ionization history of the IGM.

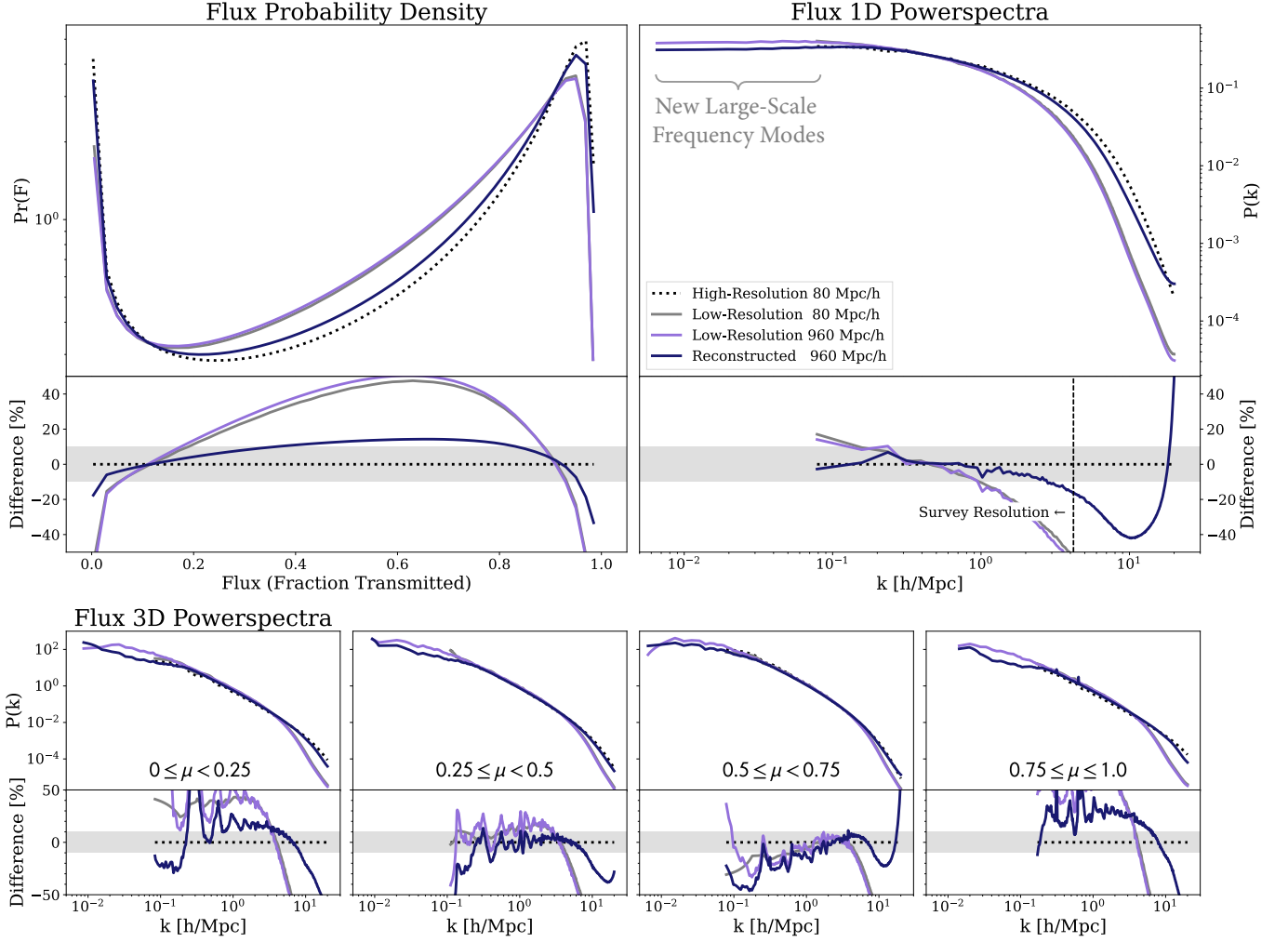


Figure 7. The Probability Density (top left panel) and Power Spectrum (top right panel) of Ly- α flux in Redshift space in four cases: the high and low-resolution Nyx simulations, the resized target, and our network output. The lower row shows the dimensionless 3D flux power spectrum in 4 μ bins. The top left is mostly parallel to the line of sight, and the bottom right panel shows the power spectrum mostly perpendicular to the line of sight. The grey band in the residual highlights the 10% error range around our machine-learned reconstructed large box. Our output (in blue) shows clear improvement over the low-resolution Nyx simulation (in grey).

4.2. Lyman-alpha Fields

The most commonly used statistics for extracting information about cosmology from maps of Lyman- α flux are the power spectrum ($P(k)$) and probability density function (PDF). These statistics are calculated using the `gimlet` code (Friesen et al. 2016) along sightlines or “skewers” that pass through the entire volume, parallel to one of the axes, simulating a random distribution of quasar spectra which probe our simulated fields.

The probability density function, $Pr(F)$ is defined such that the integral of P over the full range of F is equal to 1, $\int_0^1(F)dF = 1$. We show the PDF of our model’s Ly α predictions compared against that of the high-res and low-res simulations in Figure 7. We find that the PDF of our reconstructed Ly- α is within about

10% of the true values and thus offers a substantial improvement over the low-resolution simulation, whose PDF is off by as much as 50% in some places.

The power spectrum of the Ly- α forest offers a promising route to measuring both the properties of the IGM and cosmological parameters. The 1D Power Spectrum (P1D) is one of the most important observables that can be predicted by our cosmological models, it is defined as the integrated power of the Fourier transform of the Ly- α Flux overdensity, as a function of wavenumber. We plot the mean power spectrum $\langle P(k) \rangle$ averaged over modes with magnitude k from all skewers, as done in Lukić et al. (2015). We show comparisons between the generated and ‘true’ P1D in Figure 7. Our reconstructed Ly- α P1D is in agreement with the

high-resolution test volume to within 10% for wavenumbers smaller than 5 h/Mpc and is in better agreement than the low-resolution simulation for all wavenumbers present in the test volume.

While our machine-learning model is only able to make adjustments to the field at small scales, by construction, it is worth noticing how the total power at very large scales (ie. low wavenumbers) is affected. Our reconstruction produces a decrease of about 20% in the power contained in wavenumbers below 10^{-1} . It is currently impossible to make accurate traditional simulations of large enough scales to confirm, but we believe that difference to be principally due to our model’s correction of the mean Ly- α flux. The total power integrated over the entire spectrum must remain constant, so increasing the power contained in the small-scale modes affects the large-scale modes in this way. However, due to the highly non-linear relationship between the Ly- α flux and the density and temperature, this effect is not something that can be calculated by hand.

Finally, we present the 3D power spectrum (P3D) of the Lyman- α flux in figure 7. Unlike the hydrodynamic fields, the flux field is anisotropic along the line of sight due to redshift-space distortions. A common method of describing an anisotropic power spectrum is by measuring in terms of an angle with the line of sight, rather than integrating over spherical shells as done in the 1D power spectrum. We present the 3D power spectrum in terms of the wave-number k and the angle between the wave-vector and the line of sight, μ , defined as $\mu \equiv k_{\parallel}/|\mathbf{k}|$. We plot the D power spectrum in 4 bins with respect to μ : $[0, 0.25)$, $[0.25, 0.5)$, $[0.5, 0.75)$, $[0.75, 1]$. The later bin is most nearly parallel to the line of sight, while the first bin is almost perpendicular to the line of sight. We show the 3D power spectrum in these 4 bins in Figure 7. For all 4 μ bins, our reconstructed Ly- α achieves presents a clear improvement over the low-resolution simulations. The improvement is greatest in the 4th bin, $0.75 \leq \mu \leq 1$, where the low resolution is off by $> 50\%$ for most scales. This bin is also the most important for Ly- α forest mapping since it represents the spectral power most nearly along the line of sight, most similar to the information that is immediately available from a small sample of quasar spectra. The substantial accuracy improvements offered by our reconstructed P3D opens the door for building accurate Ly- α mock skies in Gpc volumes, using 4096^3 - 8192^3 grids. As surveys of quasar spectra become denser and the correlation of modes perpendicular to the line of sight becomes accessible (as shown in fig 9), it will become necessary to model the 3D power spectrum more accurately.

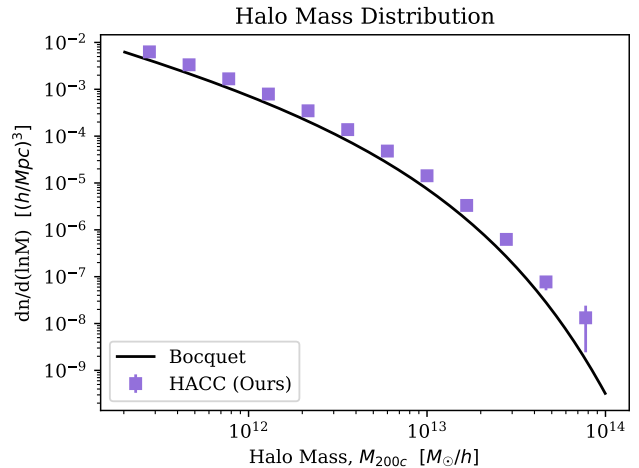


Figure 8. Halo mass function at $z = 3$ for SO halos identified in the 960 Mpc/h HACC run. The solid black line shows the corresponding Bocquet et al. (2016) fitting function, which was calibrated to simulation results at $z \leq 2$.

4.3. Companion N-body simulation

We performed an N-body companion simulation of the 960 Mpc/h box using the Hardware/Hybrid Accelerated Cosmology Code (HACC; Habib et al. 2016). The initial white noise field of the original Nyx hydrodynamic simulation was used to generate positions and velocities of 6144^3 dark matter particles at a starting redshift of $z = 200$. The particles were subsequently evolved to $z = 3$ using gravitational forces via typical N-body methods with a Plummer softening length of 1.56 kpc/h.

Halos were identified at the final redshift using a two-step approach. First, friends-of-friends (FOF) halos were identified using the ArborX library (Prokopenko et al. 2024) built into the parallel analysis framework of HACC. We employ a linking length of $b = 0.168$ and assign the center of each FOF halo as the location of its most bound particle. Next, spherical overdensity (SO) halos are constructed around the center position of each FOF halo using an overdensity criterion of 200 times the critical density of the universe. The mass function of SO halos at $z = 3$ is shown in Figure 8 where we also compare to the Δ_{200c} fitting function from Bocquet et al. (2016). Our mass function sits somewhat above the fitting function, but it is important to note that the latter was not calibrated to the high redshift shown here. Overall, we see that the simulation provides good sampling in nearly three orders of magnitude in halo mass. Moreover, the properties of the N-body dark matter halo catalog we present match those of smaller, state-of-the-art simulations, but our halo map spans a very large volume which will allow cosmologists to probe the history of the universe on very large scales.

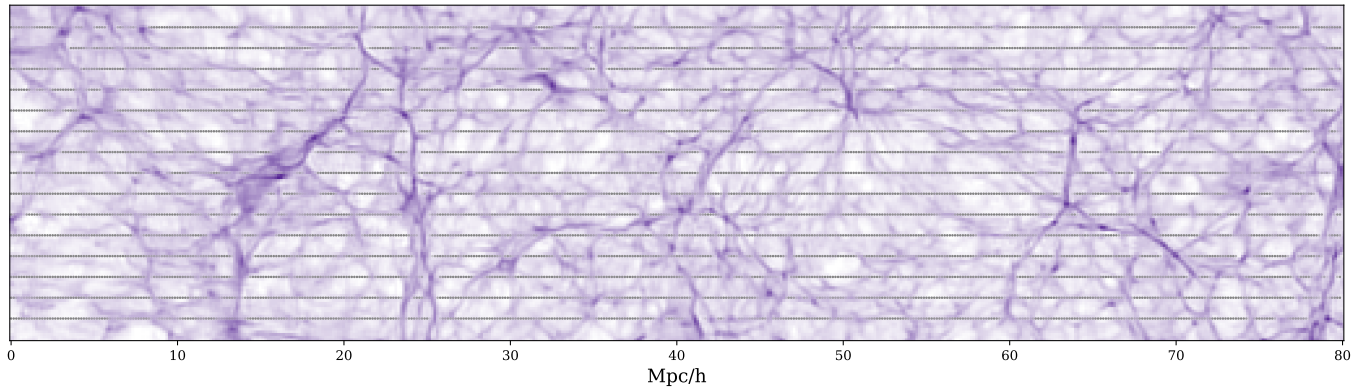


Figure 9. Visualization of a region of our simulation, with uniformly sampled quasar spectra overlaid. The (non-redshifted) Lyman- α flux is plotted here as the opacity of the points along the lines of sight. Notice that the absorption regions are correlated with other nearby lines of sight, if they pass through the same galaxy clusters.

5. CONCLUSION

In this work, we have presented a nearly Gigaparsec-wide volumetric simulation of the hydrodynamic fields and the corresponding Lyman- α flux at a redshift of $z = 3$. This volume was reconstructed from a relatively low-resolution simulation, using a deep-learning algorithm that we designed and optimized to enhance such low-resolution simulations. We have demonstrated that this translation provides an accurate reconstruction over a wide range of scales down to ~ 0.1 Mpc/h, captures a number of important statistical properties, and outperforms the low-resolution input simulation in all regimes. Our method provides a far less computationally expensive way to produce volumes like this one of incredibly large scales. Our network can be conveniently trained on a relatively small volume for some given cosmological and astrophysical parameters and then used to reconstruct an arbitrarily large volume. As shown in Figure 5, even an 80 Mpc/h sample is sufficient to accurately train the model. Our method has allowed us to produce a mock universe over 1000 times larger than the state-of-the-art simulations currently being used to calibrate surveys like DESI (Walther et al. 2021).

We have shown that, due to the highly non-linear nature of the Lyman- α forest, it is necessary to correct inaccuracies at very small scales as they will affect the spectral statistics at very large scales, demonstrating the need for approaches like ours. The very large-scale correlations (of 100 Mpc or larger) will allow us to probe the history of the universe at unprecedented early times (Seljak et al. 2005) and it is critical that we model these features accurately. We therefore cannot use traditional numerical simulations only, as they are either computationally unaffordable or their resolutions are too poor to accurately reproduce the spectral statistics of the Lyman- α forest at any scale (as shown in figure 7).

We have also produced a corresponding N-body dark matter Halo map with a statistically accurate halo population and which was generated using the same cosmological parameters and initial conditions as our hydrodynamic volume. The combination of these two volumes will allow cosmologists to explore the rich cross-correlations between the Lyman- α forest and galaxy halo maps and develop new statistical tools for extracting physical insight from surveys of the cosmos.

There are some notable shortcomings in the hydrodynamic field reconstructions, particularly in and around the larger clusters and shocks. While these regions represent a very small percentage of the universe by volume and have only a marginal effect on the Ly- α statistics, they are of significant astrophysical interest and affect the hydrodynamic statistics shown in figure 6. Because these regimes are especially dependent on sub-grid dynamics, they are poorly captured by the input low-resolution simulation and present the greatest challenge to our machine learning model. However, our technique presents a significant improvement over others at capturing these shocks and accurately reproducing the statistics of the Ly- α forest.

6. ACKNOWLEDGMENTS

This work was partially supported by the DOE’s Office of Advanced Scientific Computing Research and Office of High Energy Physics through the Scientific Discovery through Advanced Computing (SciDAC) program. This research used resources of the National Energy Research Scientific Computing Center, a DOE Office of Science User Facility supported by the Office of Science of the U.S. Department of Energy under Contract No. DEC02-05CH11231. This research also used resources of the Argonne Leadership Computing Facility, which is a DOE Office of Science User Facility supported under Contract DE-AC02-06CH11357.

REFERENCES

- Almgren, A. S., Bell, J. B., Lijewski, M. J., Lukić, Z., & Andel, E. V. 2013, *The Astrophysical Journal*, 765, 39, doi: [10.1088/0004-637x/765/1/39](https://doi.org/10.1088/0004-637x/765/1/39)
- Armengaud, E., Palanque-Delabrouille, N., Yèche, C., Marsh, D. J. E., & Baur, J. 2017, *Monthly Notices of the Royal Astronomical Society*, 471, 4606, doi: [10.1093/mnras/stx1870](https://doi.org/10.1093/mnras/stx1870)
- Baur, J., Palanque-Delabrouille, N., Yèche, C., et al. 2017, *Journal of Cosmology and Astroparticle Physics*, 2017, 013, doi: [10.1088/1475-7516/2017/12/013](https://doi.org/10.1088/1475-7516/2017/12/013)
- Blas, D., Lesgourgues, J., & Tram, T. 2011, *JCAP*, 2011, 034, doi: [10.1088/1475-7516/2011/07/034](https://doi.org/10.1088/1475-7516/2011/07/034)
- Bocquet, S., Saro, A., Dolag, K., & Mohr, J. J. 2016, *MNRAS*, 456, 2361, doi: [10.1093/mnras/stv2657](https://doi.org/10.1093/mnras/stv2657)
- Boera, E., Becker, G. D., Bolton, J. S., & Nasir, F. 2019, *ApJ*, 872, 101, doi: [10.3847/1538-4357/aafec4](https://doi.org/10.3847/1538-4357/aafec4)
- Cen, R., Miralda-Escudé, J., Ostriker, J. P., & Rauch, M. 1994, *ApJL*, 437, L9, doi: [10.1086/187670](https://doi.org/10.1086/187670)
- Chabanier, S., Palanque-Delabrouille, N., Yèche, C., et al. 2019, *JCAP*, 2019, 017, doi: [10.1088/1475-7516/2019/07/017](https://doi.org/10.1088/1475-7516/2019/07/017)
- Chabanier, S., Emberson, J. D., Lukić, Z., et al. 2023, *MNRAS*, 518, 3754, doi: [10.1093/mnras/stac3294](https://doi.org/10.1093/mnras/stac3294)
- Chiang, C.-T., & Slosar, A. 2018, *JCAP*, 2018, 012, doi: [10.1088/1475-7516/2018/01/012](https://doi.org/10.1088/1475-7516/2018/01/012)
- Chou, A. S., Soares-Santos, M., Tait, T. M. P., et al. 2022, arXiv e-prints, arXiv:2211.09978, doi: [10.48550/arXiv.2211.09978](https://doi.org/10.48550/arXiv.2211.09978)
- Croft, R. A. C., Weinberg, D. H., Pettini, M., Hernquist, L., & Katz, N. 1999, *ApJ*, 520, 1, doi: [10.1086/307438](https://doi.org/10.1086/307438)
- Dash, C. B. V., & Guha Sarkar, T. 2021, *JCAP*, 2021, 016, doi: [10.1088/1475-7516/2021/02/016](https://doi.org/10.1088/1475-7516/2021/02/016)
- DESI Collaboration, Aghamousa, A., Aguilar, J., et al. 2016, arXiv e-prints, arXiv:1611.00036, <https://arxiv.org/abs/1611.00036>
- Doughty, C. C., Hennawi, J. F., Davies, F. B., Lukić, Z., & Oñorbe, J. 2023, arXiv e-prints, arXiv:2305.16200, doi: [10.48550/arXiv.2305.16200](https://doi.org/10.48550/arXiv.2305.16200)
- Dvorkin, C., Blum, K., & Kamionkowski, M. 2014, *PhRvD*, 89, 023519, doi: [10.1103/PhysRevD.89.023519](https://doi.org/10.1103/PhysRevD.89.023519)
- Friesen, B., Almgren, A., & Lukić, Z. 2016, *Comput. Astrophys.*, 2, <https://doi.org/10.1186/s40668-016-0017-2>
- Garny, M., Konstandin, T., Sagunski, L., & Tulin, S. 2018, *JCAP*, 2018, 011, doi: [10.1088/1475-7516/2018/09/011](https://doi.org/10.1088/1475-7516/2018/09/011)
- Goodfellow, I., Pouget-Abadie, J., Mirza, M., et al. 2014, in *Advances in Neural Information Processing Systems*, ed. Z. Ghahramani, M. Welling, C. Cortes, N. Lawrence, & K. Weinberger, Vol. 27 (Curran Associates, Inc.), <https://proceedings.neurips.cc/paper/2014/file/5ca3e9b122f61f8f06494c97b1afccf3-Paper.pdf>
- Habib, S., Pope, A., Finkel, H., et al. 2016, *NewA*, 42, 49, doi: [10.1016/j.newast.2015.06.003](https://doi.org/10.1016/j.newast.2015.06.003)
- Huertas-Company, M., & Lanusse, F. 2023, *PASA*, 40, e001, doi: [10.1017/pasa.2022.55](https://doi.org/10.1017/pasa.2022.55)
- Iršič, V., Viel, M., Haehnelt, M. G., Bolton, J. S., & Becker, G. D. 2017, *Physical Review Letters*, 119, 031302, doi: [10.1103/PhysRevLett.119.031302](https://doi.org/10.1103/PhysRevLett.119.031302)
- Jacobus, C., Harrington, P., & Lukić, Z. 2023, *The Astrophysical Journal*, 958, 21, doi: [10.3847/1538-4357/acfc65](https://doi.org/10.3847/1538-4357/acfc65)
- Jiang, L., Zhang, C., Huang, M., et al. 2020, in *Computer Vision – ECCV 2020*, ed. A. Vedaldi, H. Bischof, T. Brox, & J.-M. Frahm (Cham: Springer International Publishing), 206–222
- Karaçaylı, N. G., Padmanabhan, N., Font-Ribera, A., et al. 2022, *MNRAS*, 509, 2842, doi: [10.1093/mnras/stab3201](https://doi.org/10.1093/mnras/stab3201)
- Karaçaylı, N. G., Martini, P., Guy, J., et al. 2023, arXiv e-prints, arXiv:2306.06316, doi: [10.48550/arXiv.2306.06316](https://doi.org/10.48550/arXiv.2306.06316)
- Karras, T., Laine, S., & Aila, T. 2019, A Style-Based Generator Architecture for Generative Adversarial Networks. <https://arxiv.org/abs/1812.04948>
- Karras, T., Laine, S., Aittala, M., et al. 2020, Analyzing and Improving the Image Quality of StyleGAN. <https://arxiv.org/abs/1912.04958>
- Lukić, Z., Stark, C. W., Nugent, P., et al. 2015, *MNRAS*, 446, 3697, doi: [10.1093/mnras/stu2377](https://doi.org/10.1093/mnras/stu2377)
- McDonald, P., Seljak, U., Cen, R., et al. 2005, *ApJ*, 635, 761, doi: [10.1086/497563](https://doi.org/10.1086/497563)
- McQuinn, M. 2016, *ARA&A*, 54, 313, doi: [10.1146/annurev-astro-082214-122355](https://doi.org/10.1146/annurev-astro-082214-122355)
- Meer, P., Baugher, E. S., & Rosenfeld, A. 1987, *IEEE Transactions on Pattern Analysis and Machine Intelligence*, PAMI-9, 512, doi: [10.1109/TPAMI.1987.4767939](https://doi.org/10.1109/TPAMI.1987.4767939)
- Mirza, M., & Osindero, S. 2014, Conditional Generative Adversarial Nets. <https://arxiv.org/abs/1411.1784>
- Palanque-Delabrouille, N., Yèche, C., Schöneberg, N., et al. 2019, arXiv e-prints, arXiv:1911.09073, <https://arxiv.org/abs/1911.09073>
- . 2020, *JCAP*, 2020, 038, doi: [10.1088/1475-7516/2020/04/038](https://doi.org/10.1088/1475-7516/2020/04/038)

- Palanque-Delabrouille, N., Yèche, C., Borde, A., et al. 2013, *Astronomy & Astrophysics*, 559, A85, doi: [10.1051/0004-6361/201322130](https://doi.org/10.1051/0004-6361/201322130)
- Palanque-Delabrouille, N., Yèche, C., Lesgourgues, J., et al. 2015a, *Journal of Cosmology and Astroparticle Physics*, 2015, 045–045, doi: [10.1088/1475-7516/2015/02/045](https://doi.org/10.1088/1475-7516/2015/02/045)
- Palanque-Delabrouille, N., Yèche, C., Baur, J., et al. 2015b, *Journal of Cosmology and Astroparticle Physics*, 2015, 011–011, doi: [10.1088/1475-7516/2015/11/011](https://doi.org/10.1088/1475-7516/2015/11/011)
- Park, T., Liu, M.-Y., Wang, T.-C., & Zhu, J.-Y. 2019, in *Proceedings of the IEEE/CVF conference on computer vision and pattern recognition*, 2337–2346
- Planck Collaboration, Ade, P. A. R., Aghanim, N., et al. 2016, *A&A*, 594, A13, doi: [10.1051/0004-6361/201525830](https://doi.org/10.1051/0004-6361/201525830)
- Prokopenko, A., Arndt, D., Lebrun-Grandié, D., et al. 2024, *arXiv e-prints*, arXiv:2409.10743, doi: [10.48550/arXiv.2409.10743](https://doi.org/10.48550/arXiv.2409.10743)
- Ravoux, C., Karim, M. L. A., Armengaud, E., et al. 2023, *arXiv e-prints*, arXiv:2306.06311, doi: [10.48550/arXiv.2306.06311](https://doi.org/10.48550/arXiv.2306.06311)
- Rogers, K. K., & Peiris, H. V. 2020, *arXiv e-prints*, arXiv:2007.12705. <https://arxiv.org/abs/2007.12705>
- Rorai, A., Hennawi, J. F., Oñorbe, J., et al. 2017, *Science*, 356, 418, doi: [10.1126/science.aaf9346](https://doi.org/10.1126/science.aaf9346)
- Seljak, U., Makarov, A., McDonald, P., et al. 2005, *PhRvD*, 71, 103515, doi: [10.1103/PhysRevD.71.103515](https://doi.org/10.1103/PhysRevD.71.103515)
- Sexton, J., Lukic, Z., Almgren, A., et al. 2021, *Journal of Open Source Software*, 6, 3068, doi: [10.21105/joss.03068](https://doi.org/10.21105/joss.03068)
- Vallinotto, A., Viel, M., Das, S., & Spergel, D. N. 2011, *ApJ*, 735, 38, doi: [10.1088/0004-637X/735/1/38](https://doi.org/10.1088/0004-637X/735/1/38)
- Viel, M., Becker, G. D., Bolton, J. S., & Haehnelt, M. G. 2013, *Phys. Rev. D*, 88, 043502, doi: [10.1103/PhysRevD.88.043502](https://doi.org/10.1103/PhysRevD.88.043502)
- Viel, M., Lesgourgues, J., Haehnelt, M. G., Matarrese, S., & Riotto, A. 2005, *Physical Review D*, 71, 063534, doi: [10.1103/PhysRevD.71.063534](https://doi.org/10.1103/PhysRevD.71.063534)
- Walther, M., Armengaud, E., Ravoux, C., et al. 2021, *JCAP*, 2021, 059, doi: [10.1088/1475-7516/2021/04/059](https://doi.org/10.1088/1475-7516/2021/04/059)
- Walther, M., Armengaud, E., Ravoux, C., et al. 2021, *Journal of Cosmology and Astroparticle Physics*, 2021, 059, doi: [10.1088/1475-7516/2021/04/059](https://doi.org/10.1088/1475-7516/2021/04/059)
- Walther, M., Oñorbe, J., Hennawi, J. F., & Lukić, Z. 2019, *ApJ*, 872, 13, doi: [10.3847/1538-4357/aafad1](https://doi.org/10.3847/1538-4357/aafad1)
- Wang, T.-C., Liu, M.-Y., Zhu, J.-Y., et al. 2018, in *Proceedings of the IEEE Conference on Computer Vision and Pattern Recognition*
- Xu, W. L., Dvorkin, C., & Chael, A. 2018, *PhRvD*, 97, 103530, doi: [10.1103/PhysRevD.97.103530](https://doi.org/10.1103/PhysRevD.97.103530)
- Yèche, C., Palanque-Delabrouille, N., Baur, J., & Bourboux, H. d. M. d. 2017, *Journal of Cosmology and Astroparticle Physics*, 2017, 047–047, doi: [10.1088/1475-7516/2017/06/047](https://doi.org/10.1088/1475-7516/2017/06/047)
- Zel’dovich, Y. B. 1970, *A&A*, 5, 84